Self-Organization Threshold Scaling for Thermal Atoms Coupled to a Cavity

K. J. Arnold, M. P. Baden, and M. D. Barrett

Centre for Quantum Technologies and Department of Physics, National University of Singapore, 3 Science Drive 2, 117543 Singapore

(Received 18 May 2012; published 12 October 2012)

We make a detailed experimental study of the threshold for the self-organization of thermal ^{87}Rb atoms coupled to a high-finesse cavity over a range of atom numbers and cavity detunings. We investigate the difference between probing with a traveling wave and a retroreflected lattice. These two scenarios lead to qualitatively different behavior in terms of the response of the system as a function of cavity detuning with respect to the probe. In both cases, we confirm a N^{-1} scaling of the threshold with atom number.

DOI: 10.1103/PhysRevLett.109.153002 PACS numbers: 37.30.+i, 37.10.Vz, 42.50.Pq

Atoms coupled to the standing wave mode of a cavity will self-organize for a sufficiently strong transverse pumping [1]. In essence, light scattered into the cavity results in a potential that localizes the atoms to a configuration that favorably enhances collective scattering. Thus, above a threshold pump intensity, an initially uniform distribution of atoms will undergo a phase transition, spontaneously reorganizing into a lattice configuration. Self-organization was first observed for thermal atoms in the experiments of Refs. [2,3], and later with a Bose-Einstein condensate, where it was mapped to the Dicke model [4,5]. Self-organization is of particular interest as a platform for cooling, as it can be applied to all polarizable particles, including molecules [6,7]. In particular, theoretical studies have suggested cooling that has a rate independent of particle number N [1,8], in contrast to other ensemble schemes where the cooling rate decreases linearly with N [9,10]. However, numerical simulations have suggested that the threshold may scale as $N^{-(1/2)}$ instead of N^{-1} if statistical fluctuations are required to trigger the self-organization [11]. For large ensembles, an $N^{-(1/2)}$ threshold scaling places prohibitively severe constraints on the required probe power. The threshold scaling applied will therefore greatly impact the viability of self-organization as a cooling method [12].

In this Letter, we present a systematic experimental study of the self-organization threshold for ^{87}Rb atoms trapped in a high-finesse optical cavity. We directly measure the threshold behavior over a wide range of experimental parameters for two transverse probing configurations: a retroreflected lattice and a traveling wave, as shown schematically in Fig. 1. In both configurations, the atoms are trapped intracavity by a 1560-nm far-of-resonance optical trap (FORT), which locates the atoms at every second antinode of a 780-nm cavity mode. As discussed in Ref. [13], the threshold behavior depends on both the trapping configuration and the probing geometry used, resulting in a modification to the threshold equation in Ref. [11]. However, the modified equations for both cases still maintain the N^{-1} scaling within the mean field limit, which our experimental results clearly demonstrate.

The threshold conditions relevant to our system are derived in Ref. [13] under the assumption that the system is in thermal equilibrium, and that the transverse spatial extent of the atomic ensemble is large relative to the probe wavelength. For an atom-probe coupling Ω, and for detuning $\Delta = \omega_p - \omega_a$ of the probe frequency ω_p from the atomic resonance ω_a, the threshold conditions are conveniently expressed in terms of the dimensionless quantity $\mu = -\hbar\Omega^2/(\Delta k_B T)$, which is the probe trap depth relative to the atoms' thermal energy, $k_B T$. In our system, the threshold equations are given by [13]

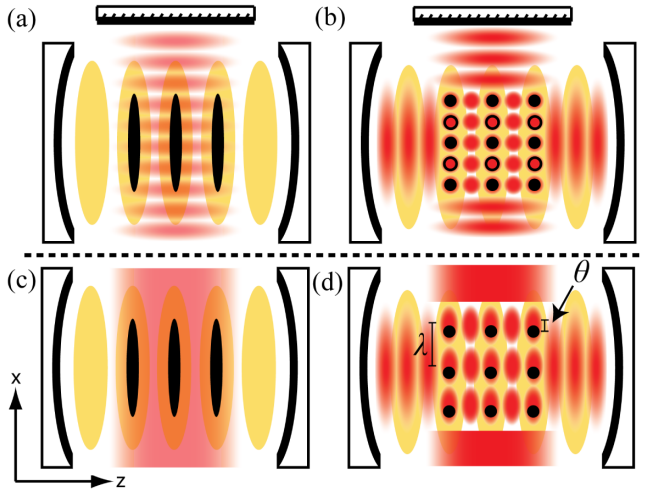

FIG. 1 (color online). Schematic representation of self-organization in the lattice (top) and traveling wave (bottom) geometry. (a),(c) Below threshold, the atoms (black) are confined by the intracavity 1560-nm FORT, indicated by light gray (yellow online). (b),(d) Above threshold, the atoms organize into a λ-spaced lattice trapped by the probe and scattered fields, indicated by dark gray (red online). (b) For a lattice probe, the atoms can form one of two possible λ-spaced lattices (filled or open circles). (d) For a traveling wave probe, interference between the probe and scattered fields results in a λ-spaced transverse lattice out of phase with the atoms by θ.

$$\left(1+\frac{I_1(\mu/2)}{I_0(\mu/2)}\right)\mu = \frac{1}{NU_0\alpha}\frac{\tilde{\Delta}_c^2+\kappa^2}{\tilde{\Delta}_c} \quad (1)$$

for the lattice geometry, and

$$\mu = \frac{\sqrt{\tilde{\Delta}_c^2+\kappa^2}}{-NU_0\alpha} \quad (2)$$

for the traveling wave geometry. In these equations, $I_k(x)$ represent the modified Bessel functions of the first kind, κ is the cavity field decay rate, and $\tilde{\Delta}_c = \Delta_c - NU_0\alpha$. In the last expression, $\Delta_c = \omega_p - \omega_c$ is the detuning of the probe frequency from the empty cavity resonance ω_c, and $NU_0\alpha$ is the dispersive shift of the cavity resonance. The dispersive shift is due to N atoms, each contributing a maximum single-atom dispersive shift $U_0 = g^2/\Delta$, where g is the atom-cavity coupling constant. The term α arises from averaging over the atomic spatial distribution. For a 1560-nm FORT, with antinodes overlapped with every other antinode of the cavity mode, as in our system, α is given by [13]

$$\alpha = \frac{1}{2}\frac{1+e^{-4/\eta}}{1+2/\eta} \quad (3)$$

where $\eta = V_{T0}/(k_B T)$ is the ratio of the trap depth, V_{T0}, to the atoms' thermal energy.

The experiments are carried out in a dual-coated high-finesse optical cavity. The cavity is 9.6 mm long and has a finesse $F = 110\,000$ near the wavelength of 780 nm and $F = 160\,000$ near 1560 nm. The high finesse at 1560 nm allows us to stabilize the length of the cavity as well as create a deep intracavity FORT. The intracavity FORT lattice has a waist of 70 μm, and is actively stabilized to a trap depth of 230 μK. The 1560 nm wavelength allows us to trap the atoms at exactly every second antinode of the 780-nm probe field, such that all trap sites are identically coupled to the cavity mode. The single-atom cooperativity is $C = g^2/\kappa\gamma \approx 6$, as determined from the cavity QED parameters $(g, \kappa, \gamma) = 2\pi \times (1.1, 0.073, 3.0)$ MHz, where g is the single-atom coupling constant for the $|F = 2\rangle$ to $|F' = 3\rangle$ cycling transition of the ^{87}Rb $D2$ line, κ is the cavity field decay rate, and γ is the atomic dipole decay rate [14].

To load atoms into the cavity, we start from a magneto-optical trap 15 mm above the cavity. We load up to 8×10^6 atoms into a single-beam 1064-nm-wavelength FORT, similar to our previous experiments [15,16]. This FORT beam is moved down 15 mm into the cavity over one second by a translation stage. Once in the cavity, the 1064-nm FORT is adiabatically ramped off, transferring the atoms into the intracavity 1560-nm FORT. By varying the number of magneto-optical trap, we control the number of atoms delivered to the cavity FORT, up to a maximum of 7×10^5.

We probe the atoms with linearly polarized light that is aligned transverse to the cavity axis, as is a magnetic field determining the quantization axis. The experiments were performed at two probe detunings from the $D2$ transition, -110 GHz and -265 GHz. The atoms are optically pumped into the $|F = 1\rangle$ ground-state manifold, resulting in a random distribution of $|m\rangle$ states. However, with these detunings and polarization, the distribution across magnetic sublevels is of no consequence.

To verify the threshold equations, we need to measure the dispersive shift and the threshold intensity. The dispersive shift is nondestructively measured by sweeping the frequency of a weak probe beam coupled to the cavity over the cavity resonance and observing the cavity transmission. Operating at a known laser-cavity detuning Δ_c, we are able to infer the dispersively shifted detuning $\tilde{\Delta}_c$ from the directly measured dispersive shift $NU_0\alpha$. Next, the threshold is measured by linearly ramping up the intensity of a transverse probe beam over 10 ms while monitoring the cavity output. The cavity output is fiber coupled and split between a single photon counting module (SPCM) and heterodyne detection setup. The SPCM is used for detecting weak signals, while the heterodyne detection is used to detect signals that would otherwise saturate the SPCM. The threshold for self-organization is clearly observed as a sudden increase in cavity output, as illustrated in Fig. 2(a).

In order to properly compare the measured threshold intensity to the threshold equations, three effects must be accounted for. First, the cavity has a significant birefringence separating the two linear polarization modes by 5κ. Limited optical access constrains the probe beam polarization to be misaligned by 21° with respect to the cavity mode polarization. This reduces the scattering rate into the cavity by 13%. Second, in the lattice configuration, ramping up the probe beam results in a significant temperature increase. Since this temperature increase is not observed for the traveling wave probe, it is most likely due to adiabatic compression. As the threshold parameter μ depends on the temperature at the threshold, we must calibrate this temperature increase. This is done by measuring the temperature throughout the adiabatic ramp of the probe power with the cavity far detuned from the probe in order to avoid the onset of self-organization. Third, the dispersive shift also depends on temperature via the parameter α. Thus, we compensate the measured dispersive shift using Eq. (3), taking into account the initial temperature 31 ± 2 μK, and the temperature at the threshold, as determined from the temperature calibration measurements.

For the traveling wave geometry, Fig. 2(c) shows the results of several threshold measurements at fixed probe detuning, Δ_c. By coarsely controlling the mean dispersive shift via the atom number, we sample a range of $\tilde{\Delta}_c$, such as the data set shown. The threshold parameter is obtained by scaling the probe depth at which light scatters into the cavity by the threshold temperature. The black line shows the theoretical threshold calculated *ab initio* from Eq. (2). Data sets such as Fig. 2(c) were taken at several values

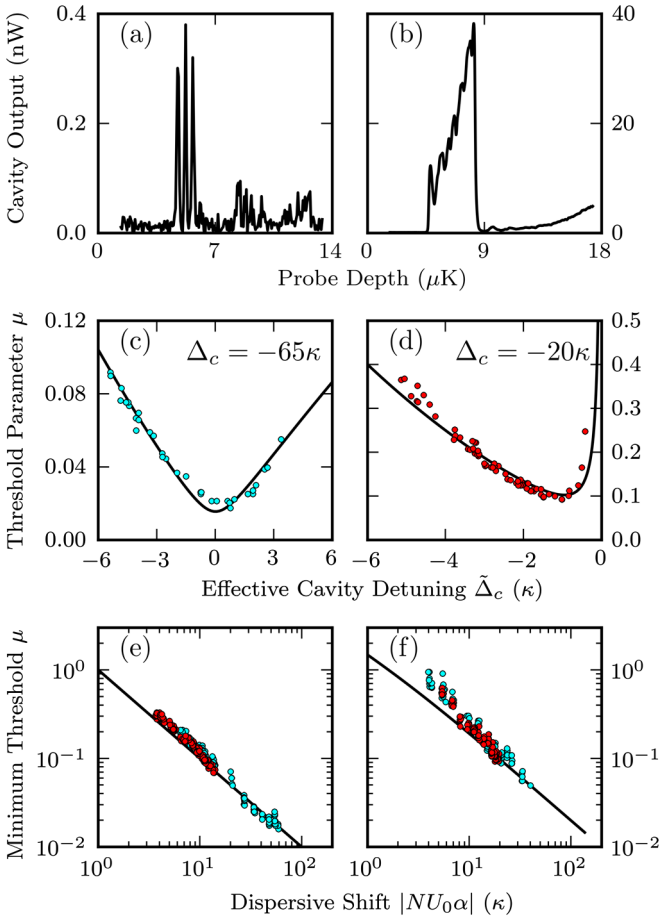

FIG. 2 (color online). Threshold measurement results for the traveling wave and lattice probe geometries, in the left and right columns, respectively. Top: The self-organization threshold is determined from the sudden increase in cavity transmission as the probe intensity is ramped up over 10 ms; example traces are shown for a traveling wave (a) and lattice (b) probe. Middle: One set of threshold measurements at fixed Δ_c, for traveling wave (c) and lattice (d) probe. The black lines are an *ab initio* calculation of the threshold from Eqs. (1) and (2) for a lattice (traveling wave) probe. Bottom: All measurements from the data sets at various Δ_c near the minimum threshold, which for the traveling wave is where $|\tilde{\Delta}_c| \leq \kappa/2$ (e), and for the lattice is where $|\tilde{\Delta}_c + \kappa| \leq \kappa/2$ (f). The black lines are the calculated minimum threshold for the respective cases. In [(c)–(f)] the black (red online) circles are data taken at the atomic detuning -265 GHz, and gray (cyan online) circles at -110 GHz.

of Δ_c, ranging from -65κ to -5κ. In Fig. 2(e), the black line shows the minimum threshold calculated from Eq. (2) at $\tilde{\Delta}_c = 0$ and all the measurements near the minimum for which $|\tilde{\Delta}_c| < \kappa/2$. As can be seen from the figures, the threshold measurements are in good agreement with Eq. (2) and a N^{-1} scaling.

For the lattice geometry, the probe beam is retroreflected, but we otherwise measure the threshold in the same way as for the traveling wave case. Figure 2(d) shows an example data set at fixed Δ_c. The black lines are calculated from Eq. (1), where the minimum threshold occurs at $\tilde{\Delta}_c = -\kappa$, in contrast to the traveling wave case. Figure 2(f) shows all the measurements near the minimum threshold, for which $|\tilde{\Delta}_c + \kappa| < \kappa/2$. Again, the results are in reasonable agreement with Eq. (1) and a N^{-1} scaling.

However, in the lattice configuration, there is an increasing discrepancy as the threshold parameter μ increases. We believe this to be a consequence of our trapping geometry. Because the 1560-nm FORT restricts the axial motion of the atoms, the probe lattice itself acts as a potential barrier that the atoms must overcome in order to organize. Clearly, in a limit in which $\mu \gg 1$ and the axial confinement is large, the atoms will not be able to organize at all. However, we observe a significant slowdown in the transition to the organized phase near the threshold even for μ approaching unity. We suspect that the organization is initially limited by the time required for the scattered potential to reduce the barrier induced by the probe and facilitate a runaway self-organization. This is supported by the observation that organization becomes rapid again if the probe intensity is well above the threshold. These effects result in the deviation of the measured threshold in Fig. 2(f) as μ approaches unity. When we ramp the probe intensity, the slow onset of self-organization near the threshold results in a delay between crossing the threshold and detecting a significant cavity output. Thus, the threshold intensity is systemically overestimated. If the atoms were not confined in the axial direction, we would expect rapid self-organization to occur for $\mu \geq 1$. The absence of any systematic deviation in the traveling wave case, as seen in Fig. 2(e), is consistent with this expectation. In this case, there is no lattice potential prior to the organization, and therefore the atoms are not confined in the transverse direction.

After the onset of self-organization, the cavity transmission traces, for example, Figs. 2(a) and 2(b) indicate complex dynamics for both probe geometries. In the case of the lattice probe configuration, our external potential geometry restricts us to $\mu < 1$ for the reasons discussed above, and we must therefore operate in the regime of large dispersive shift ($|NU_0\alpha| \gg \kappa$). In this regime, a small change in $NU_0\alpha$ results in a significant change in $\tilde{\Delta}_c$. This results in nonlinear dynamics above the threshold, owing to strong inter-dependence of the T, α, $\tilde{\Delta}_c$, and μ. We observe that the organized phase persists for at most several milliseconds, as it does in Fig. 2(b). We suspect that the increasing temperature results in the system falling below threshold and reverting to the unorganized phase. This is supported by the data shown in Fig. 3. Here, the lattice was held at constant power above the threshold, and the temperature was measured via ballistic expansion after probing for 0.8 ms. The hysteresis in the temperature as the scattered potential rises and falls indicates that the temperature rise is not simply because of adiabatic compression. It suggests the presence of a strong heating mechanism, possibly a result of nonadiabatic dynamics induced by the rapidly changing potential.

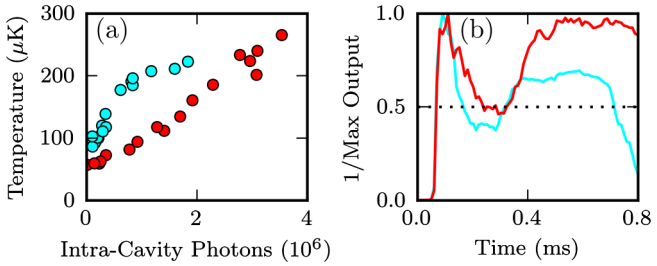

FIG. 3 (color online). Indication of excess heating due to nonadiabatic dynamics after self-organization. (a) Measured temperature after self-organization by probing above threshold at constant power for 0.8 ms plotted against the depth of the scattered field in the cavity as determined by the cavity output at the time of measurement. (b) Two example traces of the cavity output scaled the peak output corresponding to data points in (a). For the black line and circles (red online) the cavity output was above 50% of its peak at the measurement time, whereas for gray line and circles (cyan online) the transmission was already below 50% and falling. For reference, an intra-cavity photon number of 4×10^6 corresponds to a 530 μK deep optical lattice potential ($\Delta = -265$ GHz).

In the case of the traveling wave, the dynamics above the threshold are complicated by the fact that the induced organizing potential is out of phase with the atoms' positions by $\theta = \tan^{-1}(-\kappa/\tilde{\Delta}_c)$, as discussed in Ref. [13]. When $|\tilde{\Delta}_c| \lesssim \kappa$, this results in the organization switching off as the atoms are pushed away from the axial center of the cavity mode, decreasing the coupling to cavity and increasing the threshold condition. This effect can be seen from the cavity transmission trace in Fig. 2(a). Presumably, as the atoms move back into the cavity mode, self-organization is re-initiated, resulting in the observed pulsing output. In principle, the lattice can be stabilized with an additional force, as demonstrated for the collective atomic recoil lasing [17]. In our case, a displacement in the transverse Gaussian potential can counteract the phase and form a stable superradiant configuration. When $|\tilde{\Delta}_c| \gg \kappa$, only a small displacement is required since $\theta \approx 0$, and we indeed observe a stable output for several milliseconds.

In summary, we have shown that the self-organization threshold agrees well with a model based on the simple mean field considerations given in Ref. [13]. Earlier numerical work using multiparticle simulations indicated that scaling depends strongly on model details and assumptions [11]. However, we would argue that the mean field approach should yield accurate results for the threshold, provided there are sufficiently many atoms and a physical mechanism by which the atoms thermalize on the time scale of interest. In our experiments, the densities are such that collision times are $\sim$100 μs with particle numbers of $\sim 10^4$ per site of the 1560-nm lattice potential. In this case, we can expect a thermodynamic description to be valid, and therefore, the mean field results apply, as evidenced by our measurements. For cases in which a thermodynamic description may not apply, such as for fermions or low densities of molecules where the collision rate is negligible, a sub-N^{-1} scaling of the effective threshold may still be applicable.

Our experiments also indicated a strong heating mechanism above the threshold, contrary to the cooling seen in the numerical simulations [11] but consistent with the statements made in Ref. [8]. In our case, the heating is most likely due to the complex dynamics involved as the atoms organize. In future experiments, we will use a transverse 1560-nm lattice to confine the atoms. This will enable us to work more effectively in the regime of small dispersive shifts and to explore the recent theoretical proposals for dissipation-induced self-organization [8]. Additionally, we will be able to establish a two-dimensional λ-lattice. In this configuration, the atoms are expected to scatter superradiantly without threshold into the cavity mode. In this context, we can study potential cavity cooling mechanisms using weaker pumping and without the complex dynamics of the optomechanical forces driving the self-organized phase.

We acknowledge the support to this study by the National Research Foundation and the Ministry of Education of Singapore, as well as by A-STAR under Project No. SERC 052 123 0088.

[1] P. Domokos and H. Ritsch, Phys. Rev. Lett. **89**, 253003 (2002).
[2] H. W. Chan, A. T. Black, and V. Vuletić, Phys. Rev. Lett. **90**, 063003 (2003).
[3] A. Black, H. Chan, and V. Vuletić, Phys. Rev. Lett. **91**, 203001 (2003).
[4] K. Baumann, C. Guerlin, F. Brennecke, and T. Esslinger, Nature (London) **464**, 1301 (2010).
[5] D. Nagy, G. Szirmai, and P. Domokos, Eur. Phys. J. D **48**, 127 (2008).
[6] W. Lu, Y. Zhao, and P. F. Barker, Phys. Rev. A **76**, 013417 (2007).
[7] T. Salzburger and H. Ritsch, New J. Phys. **11**, 055025 (2009).
[8] W. Niedenzu, T. Grießer, and H. Ritsch, Europhys. Lett. **96**, 43 001 (2011).
[9] M. G. Raizen, J. Koga, B. Sundaram, Y. Kishimoto, H. Takuma, and T. Tajima, Phys. Rev. A **58**, 4757 (1998).
[10] P. Horak and H. Ritsch, Phys. Rev. A **64**, 033422 (2001).
[11] J. K. Asbóth, P. Domokos, H. Ritsch, and A. Vukics, Phys. Rev. A **72**, 053417 (2005).
[12] B. L. Lev, A. Vukics, E. Hudson, B. Sawyer, P. Domokos, H. Ritsch, and J. Ye, Phys. Rev. A **77**, 023402 (2008).
[13] K. J. Arnold, M. P. Baden, and M. D. Barrett, arXiv:1208.4259v1.
[14] D. A. Steck, Rubidium 87 D Line Data, http://steck.us/alkalidata (revision 2.1.4, 23 December 2010).
[15] K. J. Arnold and M. D. Barrett, Opt. Commun. **284**, 3288 (2011).
[16] K. J. Arnold, M. P. Baden, and M. D. Barrett, Phys. Rev. A **84**, 033843 (2011).
[17] D. Kruse, C. von Cube, C. Zimmermann, and P. W. Courteille, Phys. Rev. Lett. **91**, 183601 (2003).